How does the phytoplankton-light feedback affect the marine N_2O inventory?

Sarah Berthet [1*], Julien Jouanno [2], Roland Séférian [1], Marion Gehlen [3], William Llovel [4]

[1] CNRM, Université de Toulouse, Météo-France, CNRS, Toulouse, France

[2] LEGOS, Université de Toulouse, IRD, CNRS, CNES, UPS, Toulouse, France

[3] LSCE, Université Paris-Saclay, Institut Pierre Simon Laplace, Gif-Sur-Yvette, France

[4] LOPS, CNRS/University of Brest/IFREMER/IRD, Brest, France

([*]correspondence: sarah.berthet@meteo.fr)

Abstract

The phytoplankton-light feedback (PLF) describes the interaction between phytoplankton biomass and the downwelling shortwave radiation entering the ocean. The PLF allows to simulate differential heating across the ocean water column as a function of phytoplankton concentration. Only one third of the Earth system models contributing to the 6th phase of the Coupled Model Intercomparison Project (CMIP6) includes a complete representation of the PLF. In other models, the PLF is approximated either by a prescribed climatology of chlorophyll or not represented at all. Consequences of an incomplete representation of the PLF on the modelled biogeochemical state have not yet been fully assessed and remain a source of multi-model uncertainty in future projection. Here, we evaluate within a coherent modelling framework how representations of the PLF of varying complexity impact ocean physics and ultimately marine production of nitrous oxide (N_2O), a major greenhouse gas. We exploit global sensitivity simulations at 1-degree of horizontal resolution over the last two decades (1999-2018) coupling ocean, sea ice and marine biogeochemistry. The representation of the PLF impacts ocean heat uptake and temperature of the first 300 meters of the tropical ocean. Temperature anomalies due to an incomplete PLF representation drive perturbations of ocean stratification, dynamics and oxygen concentration. These perturbations translate into different projection pathways for N_2O production depending on the choice of the PLF representation. The oxygen concentration in the North Pacific oxygen minimum zone is overestimated in model runs with an incomplete representation of the PLF which results in an underestimation of local N_2O production. This leads to important regional differences of sea-to-air N_2O fluxes: fluxes are enhanced by up to 24% in the south Pacific and south Atlantic subtropical gyres, but reduced by up to 12% in oxygen minimum zones of the northern hemisphere. Our results based on a global ocean-biogeochemical model at CMIP6 state-of-the-art shed light on current uncertainties in modelled marine nitrous oxide budgets in climate models.

Plain language summary

Phytoplankton absorbs the solar radiation entering the ocean surface, and contributes to keep the associated energy in surface waters. This natural effect is either not represented in the ocean component of climate models, or in a simplified manner. We show that an incomplete representation of this biophysical interaction affects the way climate models simulate ocean warming, which leads to uncertainties in projections of oceanic emissions of an important greenhouse gas called the nitrous oxide.

Key-words: phytoplankton-light interaction; bio-physical feedback; nitrous oxide; N_2O; CMIP6 Earth system models; CNRM-ESM2-1; ocean-biogeochemical model; greenhouse gazes; marine emission; climate

Key points:

- forced ocean-biogeochemical simulations reveal that marine production of nitrous oxide is sensitive to the representation of the phytoplankton-light feedback
- the phytoplankton-light feedback perturbs the accumulation of heat and the ocean dynamics which drive changes in nitrous oxide production patterns
- an incomplete phytoplankton-light feedback overestimates sea-to-air N_2O fluxes by up to 24% in subtropical gyres and reduces them by up to 12% in oxygen minimum zones

1. Introduction

Feedbacks between the physical, biogeochemical, or ecosystem components of the ocean can trigger abrupt system changes (Heinze et al., 2021). At present the interactive phytoplankton-light feedback (PLF) is the only coupling in Earth system models between modelled marine biogeochemistry and ocean dynamics (Séférian et al., 2020). It implies that the chlorophyll (CHL) produced by the biogeochemical model is used to determine the fraction of shortwave radiation penetrating ocean surface waters. In this case, the CHL concentration profile used to approximate the influence of plankton biomass on the vertical redistribution of heat in the upper ocean is consistent with the one used to compute biogeochemical cycling.

a) Phytoplankton-light feedback (PLF)

Since the first observational evidence on how suspended matter in surface waters will impact light absorption by the ocean and change the radiative imbalance within the mixed layer (Kahru et al. 1993), this biophysical interaction has been gradually included to ocean models. Gildor and Naik (2005) highlighted the importance of considering monthly variations of CHL to capture the first-order effect of marine biota on light penetration in ocean models. Adding light-CHL interactions to numerical simulations affects oceanic processes over a wide range of spatial and temporal scales. Enabling a phytoplankton-light interaction modifies the hydrodynamics of the water column (Edwards et al., 2001; Edwards et al., 2004), the intensity of the spring-bloom in subpolar regions (Oschlies, 2004), the maintenance of the Pacific Cold Tongue (Anderson et al., 2007), the seasonality of the Arctic Ocean (Lengaigne et al., 2009), the strength of the tropical Pacific annual cycle, as well as the ENSO variability (Timmermann and Jin, 2002; Marzeion et al., 2005), the northward extension of the meridional overturning circulation (Patara et al., 2012) and the cooling of the Atlantic and Peru-Chili upwelling systems (Hernandez et al., 2017, Echevin et al., 2022).

However, the mean effect of the PLF on sea surface temperature has been argued to depend on the numerical framework (forced ocean versus coupled ocean-atmosphere models). The conflicting results reported in the literature were mainly due to diverging bio-optical protocols among models rather than to the inclusion of air-sea coupling. According to Park et al. (2014) atmosphere-ocean coupling amplifies the magnitude of PLF-induced changes, without altering the sign of the response obtained in ocean-only simulations. Two main causes were put forward to explain the sign of the final heat perturbation: either an indirect dynamical response (Murtugudde et al., 2002; Löptien et al., 2009) or a direct thermal effect (Mignot et al., 2013; Hernandez et al., 2017). Hernandez et al. (2017) further distinguished a local from a remote thermal effect by highlighting the important role played by the advection of offshore CHL-induced cold anomalies in the Benguela upwelling waters. The interplay of these mechanisms is regionally variable (Park et al., 2014). Despite the diversity of modelled responses, a consensus emerges on the first order effect of PLF on the ocean physics, which is to perturb the ocean thermal structure (Nakamoto et al., 2001; Murtuggude et al., 2002; Oschlies, 2004; Manizza et al., 2005, 2008; Anderson et al., 2007; Lengaigne et al., 2007; Gnanadesikan and Anderson, 2009; Löptien et al., 2009; Patara et al., 2012; Mignot et al., 2013; Hernandez et al., 2017). By trapping more heat at the ocean surface in eutrophic regions, such as coastal or equatorial upwellings areas, the presence of phytoplankton initially increases the surface warming. Confining heat at the surface leads to less heat penetrating in subsurface. In some cases, the advection and upwelling of subsurface cold anomalies can lead to remote cooling effects (Hernandez et al., 2017; Echevin et al., 2022). Dynamical readjustment in response to perturbations in thermal structure has also been shown to have a cooling effect, by increasing upwelling of cold water to the ocean surface (Manizza et al. 2005; Marzeion et al., 2005; Nakamoto et al., 2001; Löptien et al., 2009; Lengaigne et al., 2007; Park et al., 2014). Because these effects depend on upper ocean stratification, an important role is attributed to modelled seasonal deepening of the mixed layer as it determines the intensity of the underlying temperature anomaly and its vertical movement to the surface. In other terms, whatever the temporality of the causal chain, changes in the PLF representation are expected to both perturb the ocean heat uptake, and trigger perturbations of both the water column stratification and associated ocean dynamics.

b) This study: implications for N_2O budget uncertainties

Nitrous oxide (N_2O) is a major ozone-depleting substance (Ravishankara et al., 2009; Freing et al., 2012) and a potent greenhouse gas, whose global warming potential is 265-298 times that of CO_2 for a 100-year timescale (Myhre et al., 2013). The spatial coherence between marine productive areas and observed hot-spots of N_2O production leads to question the impact of an incomplete representation of the PLF on the simulated N_2O inventory. Recent observational studies highlight that N_2O production is high in low-oxygen tropical regions and cold upwelling waters (Arévalo-Martinez et al. 2018; 2020; Yang et al., 2020; Wilson et al., 2020). N_2O becomes increasingly saturated in surface waters of equatorial upwelling regions due to the upward advection of N_2O-rich waters (Arévalo-Martínez et al., 2017). Regions known to account for the most productive areas of the ocean spatially coincide with highest N_2O production: 64% of the annual N_2O flux occurs in the tropics, and 20% in coastal upwelling systems that occupy less than 3% of the ocean area (Yang et al., 2020).

Despite recent advances, a large range of uncertainties still surrounds oceanic N_2O emissions as large areas of both the open and coastal ocean remain undersampled by observations (Wilson et al., 2020). In particular, the paucity of observational data over key source regions contributes to increase uncertainties. The recent global budget of Tian et al. (2020) estimates natural sources from soils and oceans to contribute with up to 57% to the total N_2O emissions between 2007 and 2016, with the ocean flux reaching 3.4 (2.5−4.3) Tg N yr^{-1}. A large uncertainty range is associated to the ocean flux estimate, as it is based on outputs from only a small number of global ocean-biogeochemical models. Very few climate models, even in the current CMIP6 generation, include emissions (and beforehand a complete representation of N cycling) of N_2O fluxes: only 4 out of the 26 Earth system models considered in Séférian et al. (2020) simulate marine N_2O emissions.

The last generation of Earth system models projects an enhanced ocean warming in response to climate change, which is in turn expected to increase upper-ocean stratification (Sallée et al., 2021) and to contribute to greater reductions in upper-ocean nitrate and subsurface oxygen ventilation (Kwiatkowski et al., 2020). Ocean warming and deoxygenation constitute two triggers of high-probability high-impact climate tipping points (Heinze et al., 2021) and are identified as two of the main environmental factors influencing marine N_2O distributions (IPCC, 2019; Hutchins and Capone, 2022). Through its expected impacts on the upper ocean stratification, the PLF representation could further change the oceanic N_2O source by modulating the mixing between N_2O-rich water and intermediate depths, perturbing the way N_2O-rich water reaches the air-sea interface (Freing et al., 2012).

Here we investigate how an incomplete representation of the PLF leads to uncertainties in N_2O projection in an up-to-date global ocean-biogeochemical model making up the current generation of Earth system models. Section 2 describes the numerical model and the set of simulations, as well as the existing options to consider CHL modulations of the incoming shortwave radiation. Section 3 presents the effect of an interactive PLF on the ocean heat content, associated ocean stratification and dynamics, and its feedback on marine N_2O inventory. Finally, Section 4 summarizes the main results, addresses their broader implications, and discusses the future work motivated by this study.

2. Methodology

a) Configuration of the global ocean-biogeochemical model

Recent projections of future N_2O emissions contributing to intercomparison projects like CMIP6 are still based on Earth system models with a low spatial resolution (Séférian et al., 2020). For sake of coherence with CMIP biogeochemical modelling efforts, in the following we use a global ocean-biogeochemical configuration of the NEMO-PISCESv2 model (Madec, 2008; Aumont et al., 2015) at 1° of horizontal resolution. This model corresponds to the oceanic component of CNRM-ESM2-1 (Séférian et al., 2019) and is one of the few CMIP6-class models that contributed to the Global N_2O budget (Tian et al., 2020). Our modelled ocean has 75 vertical levels and the first level is at 0.5 meter depth. Vertical levels are unevenly spaced with 35 levels being in the first 300 meters of depth. Atmospheric forcings of momentum, incoming radiation, temperature, humidity, and freshwater are provided to the ocean surface by bulk formulae following Large and Yeager (2009). Details on physical configuration are given in Berthet et al. (2019). Using an ocean-only configuration allows to isolate the local response induced by the PLF by not confounding it with potential inter-basin feedbacks acting through the atmosphere.

JRA55-do atmospheric reanalysis (Tsujino et al., 2018; Tsujino et al., 2020) provided the atmospheric forcings of the ocean. The global domain was first spun-up under preindustrial conditions during several hundred years ensuring that all fields approached a quasi-steady state. The historical evolution of atmospheric CO_2 and N_2O concentrations was prescribed since

1850. To avoid the warming jump between the end of the spin-up and the onset of the reanalyses in 1958, the first 5 years of JRA55-do forcings were cycled, followed by the complete period of JRA55-do atmospheric forcing from 1958 to 2018.

b) Experimental design: three representations of the PLF

The control simulation (hereafter REF) together with the spin-up both account for a fully interactive PLF: the penetration of shortwave radiation into the ocean surface is constrained by the CHL concentration ([CHL]) produced by the PISCESv2 biogeochemical component (Figure S1, REF).

PISCESv2 (Pelagic Interactions Scheme for Carbon and Ecosystem Studies v2) is a 3D biogeochemical model which simulates the lower trophic levels of marine ecosystems (nanophytoplankton, diatoms, microzooplankton and mesozooplankton), the biogeochemical cycles of carbon and of the main nutrients (phosphate, nitrogen, iron, and silicate) along the 75 levels of our numerical ocean. A comprehensive presentation of the model is found in Aumont et al. (2015). PISCESv2 simulates prognostic 3D distributions of nanophytoplankton and diatom concentrations. The evolution of phytoplankton biomasses is the net outcome of growth, mortality, aggregation and grazing by zooplankton. Growth rate of phytoplankton mainly depends on the length of the day, depths of the mixed layer and of the euphotic zone, the mean residence time of the cells within the unlit part of the mixed layer and includes a generic temperature dependency (Eppley, 1972). Nanophytoplankton growth depends on the external nutrient concentrations in nitrogen and phosphate (Monod-like parameterizations of N and P limitations), and on Fe limitation which is modeled according to a classical quota approach. The production terms for diatoms are defined as for nanophytoplankton, except that the limitation terms also include silicate.

Light absorption by phytoplankton depends on the waveband and on the species (Bricaud et al., 1995). A simplified formulation of light absorption by the ocean is used in our experiments to calculate both the phytoplankton light limitation in PISCESv2 and the oceanic heating rate (Lengaigne et al., 2007). In this formulation, visible light is split into three wavebands: blue (400–500 nm), green (500–600 nm) and red (600–700 nm); for each waveband, the CHL-dependent attenuation coefficients, k_R, k_G and k_B, are derived from the formulation proposed in Morel and Maritorena (2001):

$$k_{WLB} = \sum_{\lambda_1}^{\lambda_2}\left(k(\lambda) + \chi(\lambda)[\mathrm{CHL}]^{e(\lambda)}\right) \tag{1}$$

where WLB means the wavelength band associated to red (R), green (G) or blue (B), and bounded by the wavelengths λ_1 and λ_2 as detailed above. $k(\lambda)$ is the attenuation coefficient for optically pure sea water. $\chi(\lambda)$ and $e(\lambda)$ are fitted coefficients which allows to determine the attenuation coefficients due to chlorophyll pigments in sea water (Morel and Maritorena, 2001).

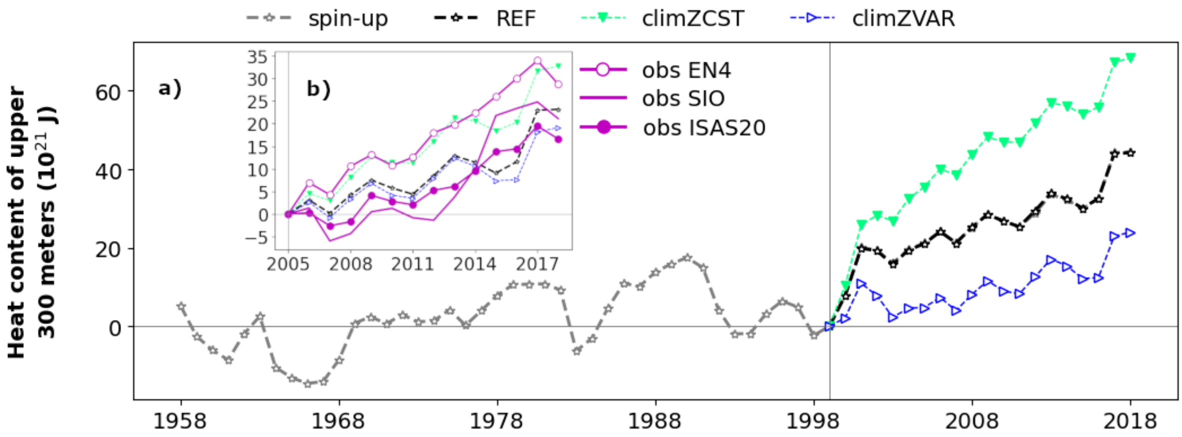

Figure 1: Modelled tropical [35°S-35°N] heat content of upper 300 m (OHC300; in ZJ) for each simulation described in Table 1: REF (black; empty stars), climZCST (green; full downward triangles) and climZVAR (blue; empty rightward triangles). In (a) final part of the spin-up has been added in gray to illustrate the branching protocol in year 1999, and OHC300 anomalies have been computed with respect to year 1999. Subplot (b) zooms over the Argo period to compare modelled tropical OHC300 anomalies with 3 in situ-based products (see section 2c).

At year 1999 two sensitivity experiments were branched off (Figure 1). Both simulations climZCST and climZVAR account for an incomplete and external PLF, as they consider an observed climatology of surface [CHL] from ESACCI (Valente et al., 2016) in order to compute the light penetration into sea water (Equation 1; Figure S1). These two simulations differ from each other by the "realism" of the vertical profile derived in each grid point from the surface value of the ESACCI CHL climatology to the level of light extinction (Table 1). climZCST uses constant profiles of CHL spreading uniformly in the vertical direction (Figure 2, b and d-f). climZVAR uses variable vertical profiles computed following Morel and Berthon (1989) (Figure 2, c and d-f). This set of simulations is representative of the several configurations used in the case of CMIP intercomparison project.

Table 1: Experimental set-up.

Simulation	Which CHL fields to interact with incoming shortwave radiation?	PLF nature
REF	uses directly the 3D CHL produced by the biogeochemical component	interactive
climZCST	uses the prescribed monthly climatology of ESACCI CHL with a constant vertical profile, equal to the value of the surface climatology up to the level of light extinction	incomplete
climZVAR	uses the prescribed monthly climatology of ESACCI CHL with a variable vertical profile, derived from the surface climatology following Morel and Berthon (1989)	incomplete

In climZCST and climZVAR, PISCESv2 prognostically simulates [CHL], a key component of biogeochemical cycles, but feedback of CHL on physics (stratification, ocean heat content) is determined by the externally prescribed [CHL] climatology. The CHL concentrations used for radiation or for biogeochemical cycles are not consistent, and phytoplankton biomass computed by the biogeochemical model does not affect the physical properties of the ocean waters.

Consequences on the marine biogeochemical mean state of incomplete representations of the PLF are assessed in the following by difference to the control run REF. This methodology allows to evaluate how different levels of realisms and complexity in resolving bio-physical interactions impact the physical and biogeochemical content of the modelled ocean. A complete description of the marine N_2O parameterization used in this model is presented in the supplementary material.

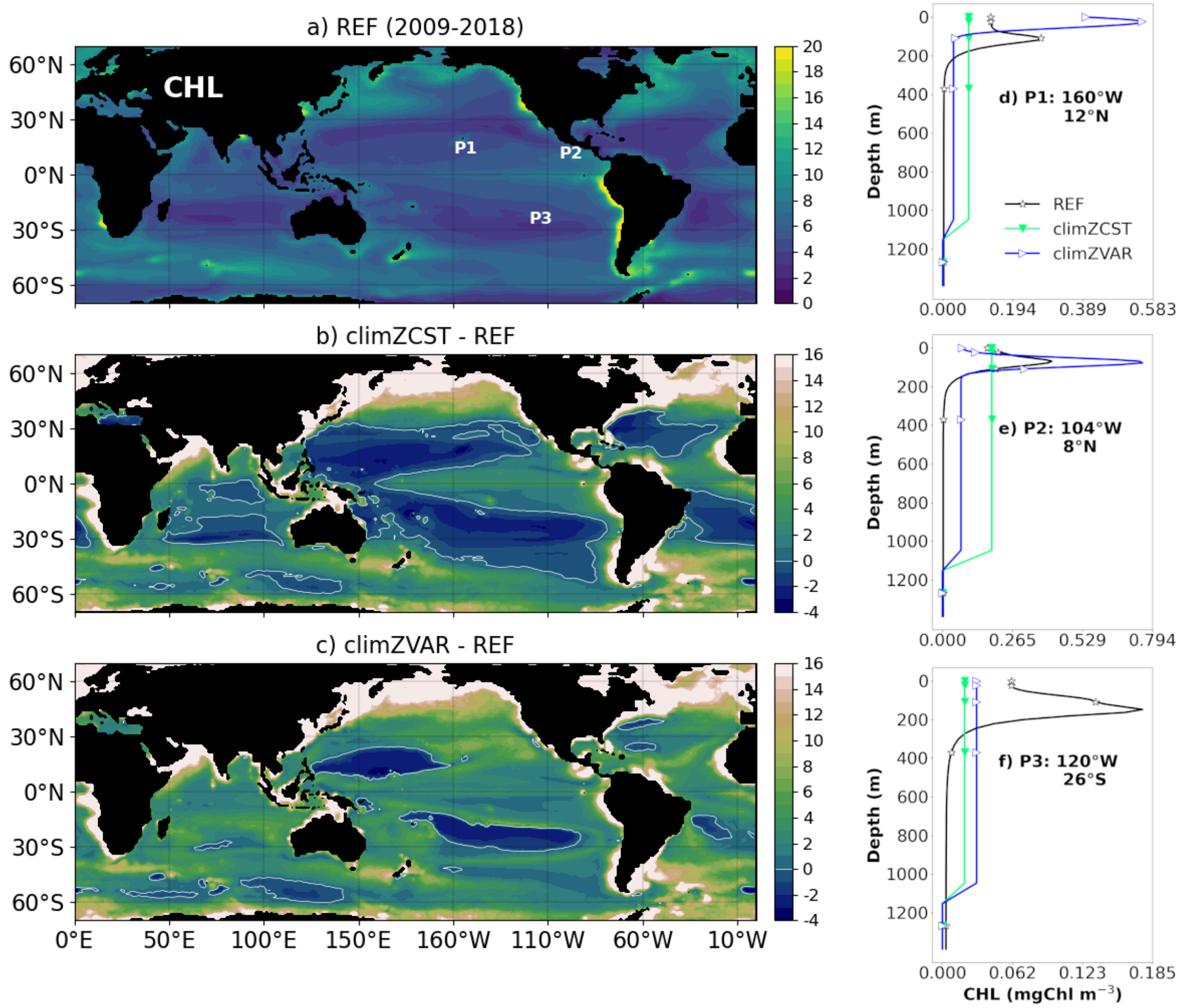

Figure 2: CHL concentration (mgCHL m^{-3}) interacting with the incoming shortwave radiation for each numerical experiment (Table 1). Maps a-c) show annual means of the vertical sum over 0-6000 m, a) as modelled over the 2009-2018 period for REF, and its differences with the external CHL prescribed for b) climZCST and c) climZVAR experiments. Labels P1 to P3 on subplot a) locate vertical profiles shown on subplots d-f).

c) Observations and analyses

Model results are compared with available observational-based gridded temperature and salinity datasets. Ocean heat content (OHC) of the upper 0-300 meter layer was inferred from three different products: i) the global objective analysis of subsurface temperature EN4 (Good et al., 2013), ii) the SIO product of the Scripps Institution of Oceanography (Roemmich anf Gilson, 2009), and iii) the ISAS20 optimal interpolation product released by Ifremer (Kolodziejczyk et al., 2019; Kolodziejczyk et al., 2021). While the SIO and ISAS20 products consider only Argo temperature and salinity profiles, the EN4 dataset considers all types of *in situ* profiles providing temperature and salinity (when available). These three *in situ*-based datasets are considered since 2005, the year the Argo coverage became sufficient to characterize the global ocean. Details on OHC computation are given in Llovel and Terray (2016) and Llovel et al. (2022). The authors also refer to cross-validations of OHC of deeper layers (0-700 m and 0-2000 m) against OHC anomalies from World Ocean Atlas 2009 (Levitus et al., 2012). A monthly climatology (1955-2012) of oceanic temperature from World Ocean Atlas 2013 version 2 (Locarnini et al., 2013) was used to evaluate modelled temperatures. Modelled O_2 was compared to the annual climatology of O_2 from World Ocean Atlas 2013 (Garcia et al., 2014) and modelled CHL was compared to the 3D monthly climatological global product estimated from merged satellite and hydrological data of Uitz et al. (2006). Modelled N_2O partial pressure difference across the air-sea interface (Dpn2o) was compared to the recent dataset of Dpn2o observations compiled by Yang et al. (2020).

In the following temporal means cover the last 10 years of simulations, from 2009 to 2018. In other analyses the whole simulated period is shown (1999-2018).

3. Results

a) Impact of PLF on the upper ocean heat content and dynamics

Meridional sections reveal that heat perturbations in response to changing CHL fields interacting with light are limited to the top 0-300 m layer of the ocean and predominantly affect the tropical area (Figure 3 and Figure S2, c-d).

The largest temperature anomalies are observed near the thermocline depth and reflect upper ocean warming and deepening of the thermocline in climZCST (Figure 3c), and cooling and shallowing of the thermocline in climZVAR (Figure 3d). In climZCST the ocean warming reflects large-scale patterns of a tropical CHL deficit compared to REF (Figure 2, b). Temperature differences are lower in the near-surface layer (0-50 m) than in the 50-300 m layer. This is expected as a result from weak stratification but also from simulations run with a forced atmosphere in which the temperature of the ocean surface layer is constrained by the atmospheric prescribed state.

When using an incomplete representation of the PLF, two contrasting trends of the upper ocean heat content (OHC) emerge compared to our control run REF (Figure 1a). Over the Argo period (2005-present) EN4 estimates of tropical OHC300 are in very good agreement with our warmest simulation climZCST (Figure 1b), while the two other dataproducts SIO and ISAS20 are in better agreement with our control run REF and with climZVAR. The good accordance between modeled OHC300 and observations is not a systematic feature of model-data comparisons (Cheng et al., 2016; Liao et al., 2022). Moreover, non-negligible differences exist among OHC dataproducts which are generally particularly strong in the upper 0-300 m layer (Lyman et al., 2010; Liang et al., 2021). The spread between these products at the end of the 2005-2018 period (12.1 10^{21} J) is comparable to that of our numerical set (13.6 10^{21} J). The modelled OHC in REF is in very good agreement with current global mean *in situ* observations (Meyssignac et al., 2019; see their Figure 11) and with OHC anomalies derived from World Ocean Atlas 2009 (Levitus et al., 2012). In accordance with these observations, our ocean-biogeochemical model simulates a global mean increase of OHC over the 2006-2016 period of order 40 10^{21} J for the upper 700 m, and of about 70 10^{21} J for the 0-2000 m layer.

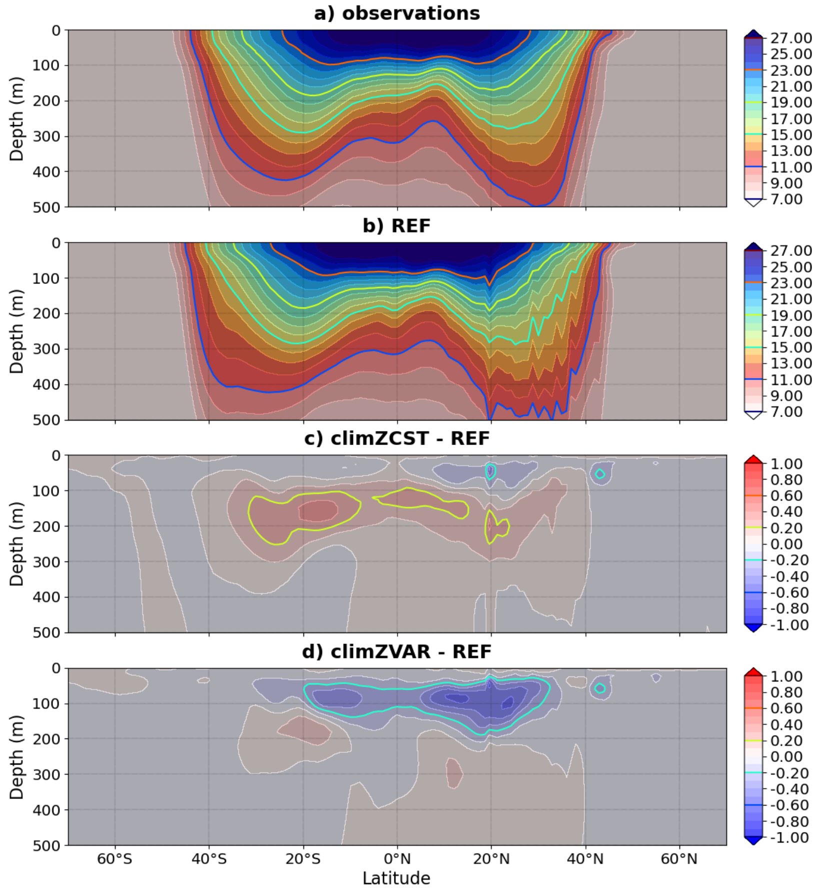

Figure 3: Mean 2009-2018 meridional section of temperature (°C) averaged over 0-360°E for a) observations, b) REF and its differences with c) climZCST and d) climZVAR.

Subsurface thermal anomalies develop rapidly (Figure S3) after branching of climZVAR and climZCST in 1999. The dipole structure of the anomaly seen in climZCST reflects the surface heat trapping in REF and the associated subsurface cooling (Figure S3, b). Indeed in climZCST the vertically constant and weaker concentrations of CHL trap less incoming shortwave than the CHL maximum seen in REF between 0 and 100 m depth (Figure 2, d-f). The negative anomaly in climZVAR suggests that the parameterization of Morel and Berthon (1989) contributes to underestimate the ocean heat uptake (Figure S3, c and Figure S2, d) compared to REF. This heat deficit results from the overestimation of the vertical integral of CHL over large areas of the tropical domain in climZVAR compared to REF (Figure 2, c). As a result, the energy associated with the incoming radiation is caught in surface waters without being distributed over the water column.

In both climZCST and climZVAR the subsurface temperature anomaly deepens progressively over the first six years of simulation as a result of vertical mixing (Figure S3). This evolution indicates that part of the OHC300 differences between simulations comes from the adjustment of climZCST and climZVAR to the spin-up mean state yielded by an interactive PLF. It can be expected that experiments having spin-ups run with different representations of the PLF, would give even stronger sensitivities than those highlighted in this study. The sensitivities of OHC300 to the PLF formulation evaluated here should be considered at the lower end of estimate of OHC discrepancies that may emerge from changing the PLF representation.

Prescribing a constant vertical profile of CHL (climZCST) to compute the penetration of the radiation into the ocean increases the OHC300 by more than 20 10^{21} J during the last two decades (1999-2018) compared to REF (Figure 1). This rise of OHC300 decreases the vertically-integrated tropical potential density of the upper 300 m at the end of the simulated period by 5 kg/m^2 compared to REF (Figure S4). The opposite trend (a reduced OHC300 compared to REF) is simulated with the same state-of-the-art CMIP6 ocean-biogeochemical model when considering a variable vertical profile of CHL (climZVAR). However Figure 1 highlights that the simulation using a consistent CHL for interacting with both incoming shortwave radiation and biogeochemical cyclings (REF) does not amplify one of these two trends, as climZCST and climZVAR surround REF. Average ranges of uncertainties associated with the PLF representation over the extended tropical domain (35°S-35°N) exceed 40 10^{21} J in terms of OHC300 (Figure 1), 4 meters for the thermocline depth and more than 9 kg/m^2 for the vertically-integrated potential density perturbation (Figure S4).

Similar to OHC300, ranges of uncertainty for the OHC estimates of deeper layers (0-700 m and 0-2000 m) also slightly exceed 40 10^{21} J. Such uncertainty ranges are quite important as they are obtained by only changing the PLF representation in a single ocean-biogeochemical model. By comparison and in the context of OMIP protocols, Tsujino et al. (2020) give spreads between CMIP model estimates of the order of 50 10^{21} J for the OHC of the upper 700m after 20 years (please refer to their Figure 24, a-b). Regarding the OHC integrated over the 0-2000m layer, they report an inter-model spread between 50 and 100 10^{21} J, depending on the OMIP protocol considered (see their Figure 24, d-e). The OHC300 uncertainty of 40 10^{21} J triggered by the representation of the PLF in our set of simulations has a comparable order of magnitude than the current spread of multi-model estimations of OHC. The present study suggests that part of the OHC multi-model uncertainty in current climate models may be due to different representations of the phytoplankton-light interaction.

The heat and associated density perturbations also cause dynamical modifications of upper ocean currents (Figure 4). Absolute differences in upper ocean velocities (average between 0 and 300m depth) are between |0.05| and |0.6| cm/s with strongest differences along the equator revealing perturbations of the equatorial undercurrent (Figure 4, b and c). Circulation around the subtropical gyres is also impacted, in particular for the South Pacific subtropical gyre. These modifications of zonal and meridional dynamics spread over the entire tropical latitudes, from 30°S to 30°N, strongly supporting the idea that heat perturbations induced by different interactions between CHL and incoming shortwave cause non-negligible modifications of the equatorial and tropical ocean dynamics.

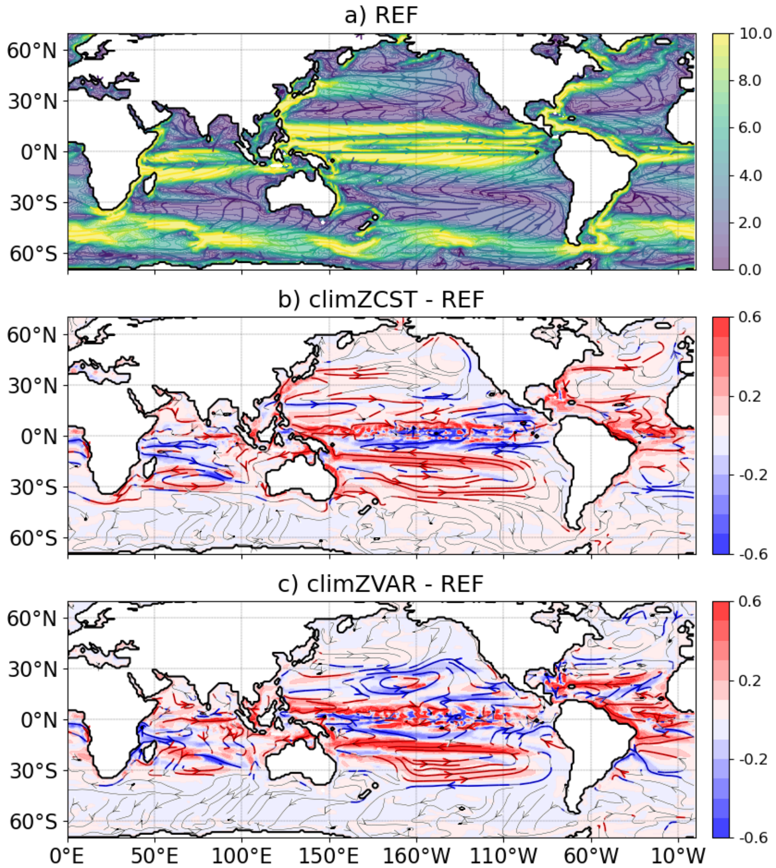

Figure 4: Annual mean speed (color; cm/s) and streamlines of oceanic currents between 0-300 m over the 2009-2018 period for a) REF, and its differences with b) climZCST and c) climZVAR. In b-c) streamlines are colored when absolute speed are larger than 0.05 cm/s.

b) PLF impact on N_2O production

Perturbations of the annual pycnocline depth (Figure 5, a-c) highlight a vertical adjustment to the heat (Figure S2) and subsequent large-scale dynamical anomalies (Figure 4). Variations of the pycnocline integrate perturbations of both thermal and salinity stratifications. However, in our simulations heat anomalies appear to drive perturbations and pycnocline depth anomalies mainly reflect those of the thermocline. The cold anomaly dominating the tropical domain in climZVAR (Figure S2, d) appears to be vertically redistributed, as it triggers an upward displacement of the isopycnals (Figure 5, c). In contrast to the anomalies seen over most of the tropical Pacific, a deepening of the isopycnals reaching up to 20 meters is modelled in both South Pacific and Atlantic subtropical gyres in climZCST and climZVAR (Figure 5, b and c). Over these subtropical gyres heat is redistributed along the vertical as the subsurface warm anomaly dives. The subduction of these heat anomalies causes in turn a deepening of the pycnocline (Figure 5, b and c). As stressed by Sweeney et al. (2005), small changes in CHL concentration (Figure S5) may have important effects on the mixed layer depth in these subtropical gyres due to low local wind speeds and low mixing conditions. This is thought to explain the large sensitivity we observe in terms of pycnocline depth (Figure 5) and ocean heat content in these regions. In line with their results, our set of simulations highlights that small CHL changes in low productivity regions trigger a vertical redistribution of density anomalies affecting the stratification.

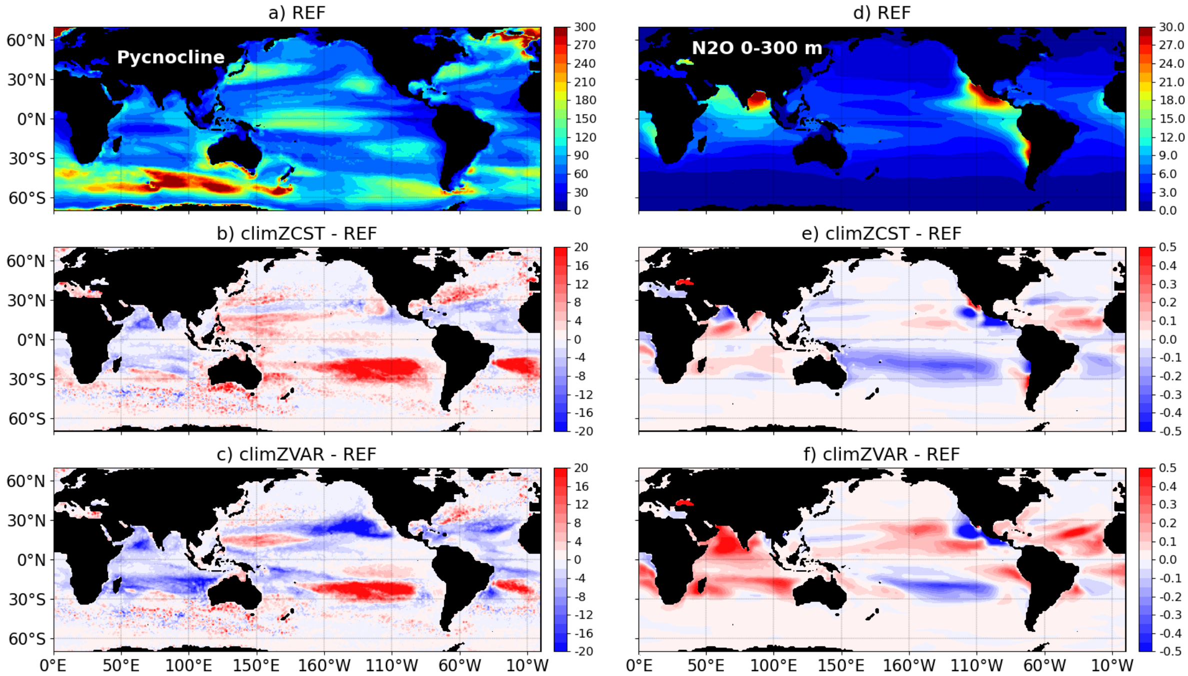

Figure 5: a-c) Depth of annual pycnocline (m) for 2009-2018 computed as the annual mean depth of the maximum of the Brunt-Väisälä frequency $N^2(T, S)$ over the water column (Maes and O Kane, 2014). d-f) Mean [N_2O] (μmolN/m^3) over the first 300 meters depth. For REF (upper panel) and its mean-state differences with climZCST (middle panel) and climZVAR (bottom panel).

Anomalies of N_2O concentration integrated over the first 300 meters of the water column (Figure 5, e and f) are in good agreement with patterns of pycnocline anomalies over the tropics (Figure 5, b and c). These comparable spatial structures attest that N_2O anomalies are driven by perturbations of stratification in large parts of the tropical domain.

In the South Pacific subtropical gyre, the concomitance of i) an increased temperature (Figure S2, c and d), ii) a reinforced transport (Figure 4, b and c) and iii) a weakened stratification illustrated by a local deepening of the pycnocline (Figure 5, b and c), contributes to decrease the N_2O concentration in both climZCST and climZVAR (Figure 5, e and f). In contrast, in the South Indian Ocean and North tropical Atlantic the increase of N_2O concentration seems to be mainly driven by the mean shoaling of the local pycnocline, as both regions exhibit contrasted perturbations in terms of transport and temperature. Finally, in the North Pacific oxygen minimum zone, the strong N_2O deficits in both climZCST and climZVAR compared to REF do not respond to stratification and transport anomalies but are rather driven by a local rise of O_2 concentration (Figure S6). Considering an incomplete PLF contributes to overestimate the oxygen concentration in this oxygen minimum zone and leads to a lack of local N_2O production.

The relationship between N_2O concentration and OHC300 in the Tropical Ocean is derived from a linear regression for each of the three 20-years simulations (Figure 6). The resulting slopes allow to identify three distinct tropical N_2O production pathways along time as a function of the oceanic heat uptake: from 0.3 µmolN m^{-2} per ZJ for the most simplified PLF scenario climZCST, to 1 µmolN m^{-2} per ZJ for climZVAR. The slope of the simulation with the higher level of realism in terms of interactivity (REF) appears a solution between the two previous extremes, as it increases its N_2O production by 0.8 µmolN m^{-2} per ZJ. Each of these N_2O production pathways will translate into a different temporal evolution of the N_2O budget and hence future climate. This result stresses the importance of having an interactive PLF in order to neither overestimate nor underestimate the N_2O production projections due to a simplified representation of the PLF.

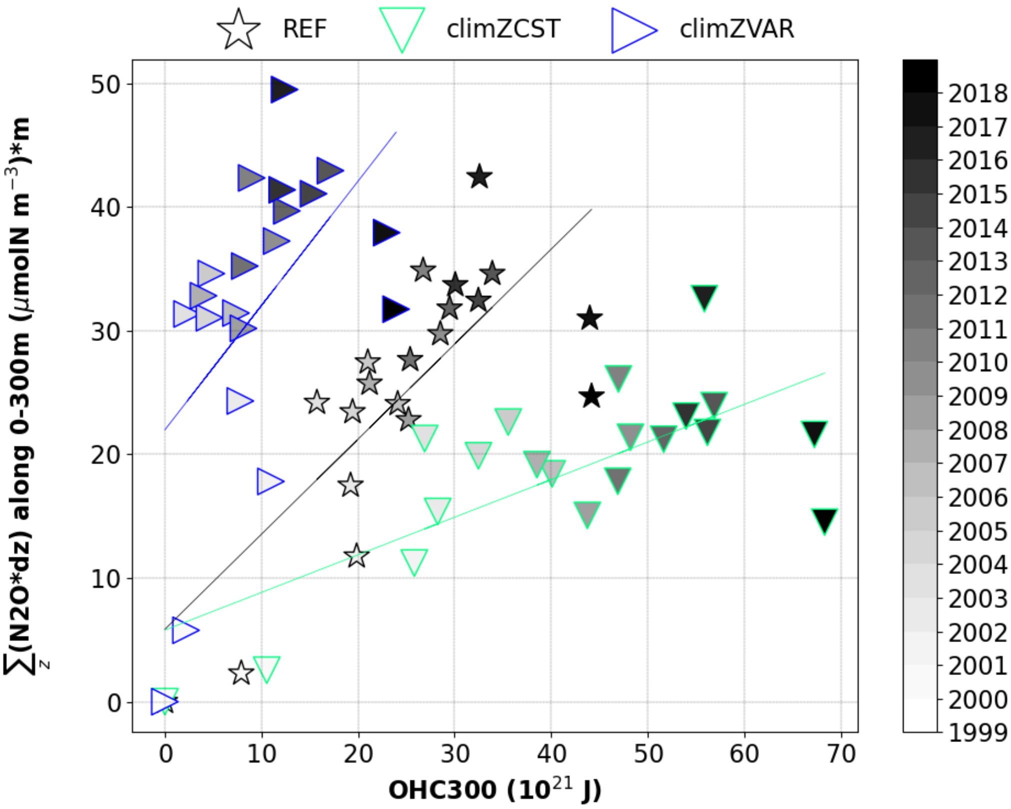

Figure 6: Annual N_2O inventory vertically integrated over the first 300 meters depth (µmolN/m^2) as a function of the annual OHC300 (ZJ) and averaged over an extended tropical domain (35°S-35°N). All points reflect anomalies compared to year 1999.

c) Impacts on oceanic N_2O emissions

By perturbing the OHC, the ocean dynamics and the N_2O production, the way PLF is modelled has non-negligible consequences on Dpn2o and thus on N_2O emissions at the air-sea interface (Figure 7). Because the atmospheric partial pressure of N_2O is identical among simulations, differences in Dpn2o are driven by changes in surface oceanic N_2O concentration normalized by those in N_2O solubility. Since solubility is mainly driven by temperature and because surface temperature anomalies are very weak (Figure S3, c and d), we do not expect solubility perturbations close to the surface. It results that spatial patterns of Dpn2o anomalies (Figure 7) reflect differences in surface oceanic N_2O concentration.

Compared to a scenario considering a fully interactive PLF (REF), an incomplete representation of the PLF underestimates Dpn2o in all oxygen minimum zones of the northern hemisphere, which are strong emission zones (Figure 7, c and d). Large Dpn2o anomalies of -2.5 natm encompasses northern parts of the oxygen minimum zones of the Indian, Pacific and Atlantic oceans and anomalies reach up to -5 natm locally. Consequently, climZCST and climZVAR underestimate N_2O fluxes by more than 12% in these oxygen minimum regions compared to REF. This result highlights that the representation of the PLF can be an important source of uncertainty in modelling N_2O fluxes. As a matter of fact, the oceanic contribution to the recent global N_2O budget by Tian et al. (2020) is based on only five global ocean-biogeochemical models (as still only few models simulate marine N_2O emissions). These models have different configurations of the PLF which adds considerable uncertainty to simulated marine N_2O emissions.

In subtropical gyres, the strong and direct effect of temperature (Figure S2, c and d) on in-depth N_2O concentration (Figure 5, e and f) is in line with Yang et al. (2020) who demonstrate that the seasonality of Dpn2o in that regions is driven by a solubility regime. Both climZCST and climZVAR overestimate Dpn2o in subtropical gyres of the South Pacific and South Atlantic (Figure 7, c and d). This leads to an overestimation of the regional N_2O fluxes by 24% compared to a simulation having a complete and interactive PLF representation (REF).

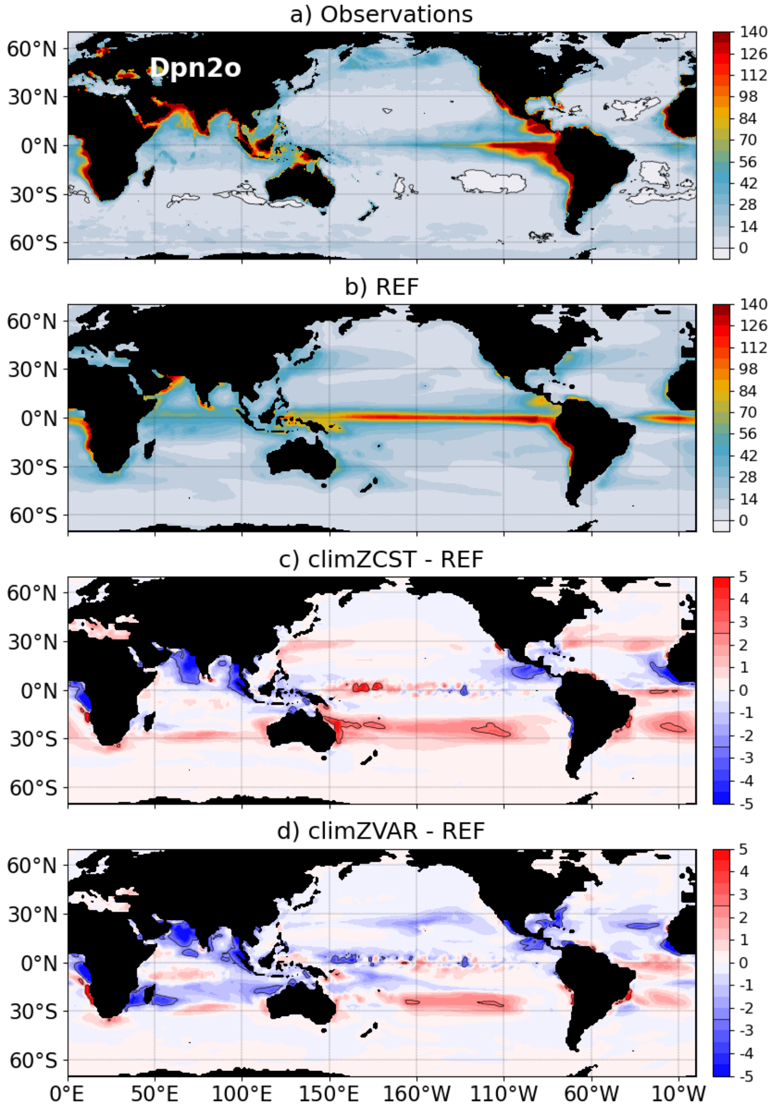

Figure 7: Mean sea-to-air Dpn2o (natm) computed from a) observations, b) REF over the 2009-2018 period, and its differences with c) climZCST and d) climZVAR compared to REF.

4. Discussion and conclusion

In this study we use the ocean component (including ocean physics, sea ice and marine biogeochemistry) of the global Earth system model CNRM-ESM2-1 which contributed to the last phase of the Coupled Model Intercomparison Project (CMIP6). Our ocean-biogeochemical model is one of the few currently able to represent an interactive phytoplankton-light feedback (PLF) by constraining the penetration of shortwave radiation into the ocean as a function of the CHL concentration produced by the biogeochemical model. Three simulations have been run at the horizontal resolution currently used for intercomparisons of Earth system models (1°). Analyses are based on differences between a control run with an interactive PLF (REF) and two experiments with an incomplete PLF (climZCST and climZVAR) using a prescribed CHL climatology to interact with the incoming solar radiation. Changing the approach to compute how CHL filters the light penetrating into the ocean highlights the consequences of using an interactive PLF.

Our results demonstrate that the approach commonly used to account for the impact of the phytoplankton on light penetration significantly interfers with upper ocean heat uptake (Figure 1), the associated dynamics (Figure 4) and stratification in the tropics (Figure 5, a-c). Our set of forced ocean-biogeochemical simulations reveals that marine production of nitrous oxide (N_2O) is sensitive to the representation of the PLF (Figure 5, d-f). The heat perturbations add to the uncertainty of modelled oceanic N_2O production and result in three N_2O production trajectories along time (Figure 6) that in turn trigger regional differences of Dpn2o and sea-air N_2O fluxes (Figure 7). Compared to an ocean model using a fully interactive PLF (REF), an incomplete PLF results in an overestimation of N_2O fluxes by up to 24% in the South Pacific and South Atlantic subtropical gyres, and a reduction by up to 12% in oxygen minimum zones of the northern hemisphere. Our results based on a model at CMIP6 state-of-the-art emphasize an overlooked important source of uncertainty in climate projections of marine N_2O production and in current estimations of the marine nitrous oxide budget.

In subtropical gyres of the southern Hemisphere which are regions of low productivity, small CHL changes have a strong and direct effect on temperature (Figure S2, c and d), transport (Figure 4, b and c) and local stratification (Figure 5, b and c). These concomittant effects result in a local decrease of N_2O concentrations in both experiments with a simplified PLF representation (climZCST and climZVAR).

In forced ocean simulations, atmospheric forcings constrain surface temperature, salinity and thus solubility. However, the N_2O concentration integrated over the upper 300 meters depth of the water column (Figure 5, e-f) showed differences with the control run that follow those of the in-depth temperature (Figure S2, c-d): in climZCST (climZVAR), a warmer (colder) tropical ocean leads to a decreased (an increased) N_2O concentration. Because higher marine greenhouse gas emissions will increase the temperature of the coupled atmosphere-ocean system, adding an interactive atmospheric component is expected to amplify the PLF-induced mean changes in marine N_2O concentration highlighted in this ocean-only numerical set (Park et al., 2014; Asselot et al., 2022).

Our results also question the reliability of current modelled estimates of the area and volume of oxygen minimum zones, as well as their trends in a future climate. The expansion rate of O_2-depleted waters still remains unclear and its controlling mechanisms are not yet fully understood and represented in today's models. Observation based assessments suggested that the ocean has already lost around 2% of the global marine oxygen since 1960 (Schmidtko et al., 2017). The expansion of oxygen minimum zones is expected to result in an increase of the volume of suboxic water and to have an impact on the production and decomposition of N_2O (Freing et al., 2012). Our set of simulations highlights that an incomplete representation of the PLF underestimates the expansion of oxygen-depleted waters over the 20 years of simulation in comparison to REF. In climZCST and climZVAR the global volume (0-1000 m) of hypoxic water with [O_2] under 50 mmol m^{-3} is up to 2.3 10^{14} m^3 lower in 2018 compared to that of the control run REF. Thus an incomplete representation of the PLF might lead to an underestimation by 1.2 % of the modelled tropical volume of low-oxygenated waters after 20 years.

Recent regional studies demonstrated that the interactive PLF strongly affects upwelling systems of the South Pacific and Atlantic oceans (Hernandez et al., 2017; Echevin et al., 2021). Coastal upwellings are known to be sites of high N_2O production with an annual N_2O flux amounting to approximately 20% of the global fluxes while these systems occupy less than 3% of the ocean area (Yang et al., 2020). However, in the present study main modelled perturbations are rather localized over oxygen minimum zones or subtropical gyres (Figure 5; Figure 7). While the latter regional studies were performed at horizontal resolutions compatible with the complex dynamics of coastal upwellings (from 10 km to about 28 km), the resolution of climate models (~1-degree of horizontal resolution) does not allow to resolve these dynamics. A step further would be to evaluate how the sensitivity of N_2O emission to the representation of the PLF depends on the horizontal resolution by running simulations at higher resolution with the same climate model. This would help to better determine how coastal upwelling systems may impact the modelled N_2O inventory through different PLF representations, as well as the associated modelled range of uncertainty.

Code availability

Sources for NEMO and PISCESv2 codes are available from https://forge.nemo-ocean.eu/nemo.

Acknowledgements

The OHC data were collected and made freely available by the International Argo Program and the national programs that contribute to it (https://argo.ucsd.edu, https://www.ocean-ops.org). The Argo Program is part of the Global Ocean Observing System. R. Séférian acknowledges the European Union's Horizon 2020 research and innovation program under grant agreement No. 101003536 (ESM2025 – Earth System Models for the Future).

References

Anderson,W. G., A. Gnanadesikan, R. Hallberg, J. Dunne, and B. L. Samuels (2007), Impact of ocean color on the maintenance of the Pacific Cold Tongue, Geophys. Res. Lett., 34, L11609, doi:10.1029/2007GL030100.

Asselot, R., Lunkeit, F., Holden, P. B., & Hense, I. (2022). Climate pathways behind phytoplankton-induced atmospheric warming. Biogeosciences, 19(1), 223-239.

Aumont, O., Ethé, C., Tagliabue, A., Bopp, L., & Gehlen, M. (2015). PISCES-v2: An ocean biogeochemical model for carbon and ecosystem studies. Geoscientific Model Development, 8, 2465–2513.

Arévalo-Martinez, D. L., A. Kock, T. Steinhoff, P. Brandt, M. Dengler, T. Fischer, A. Körtzinger, and H. W. Bange (2017), Nitrous oxide during the onset of the Atlantic cold tongue, J. Geophys. Res. Oceans, 122, 171–184, doi:10.1002/2016JC012238

Arévalo-Martínez, D. L., Steinhoff, T., Brandt, P., Körtzinger, A., Lamont, T., Rehder, G., & Bange, H. W. (2019). N2O emissions from the northern Benguela upwelling system. Geophysical Research Letters, 46, 3317–3326. https://doi.org/10.1029/2018GL081648

Berthet, S., Séférian, R., Bricaud, C., Chevallier, M., Voldoire, A., & Ethé, C. (2019). Evaluation of an online grid-coarsening algorithm in a global eddy-admitting ocean biogeochemical model. Journal of Advances in Modeling Earth Systems, 11, 1759–1783. https://doi.org/10.1029/2019MS001644

Bopp, L., Resplandy, L., Orr, J. C., Doney, S. C., Dunne, J. P., Gehlen, M., Halloran, P., Heinze, C., Ilyina, T., Séférian, R., Tjiputra, J., and Vichi, M. (2013). Multiple stressors of ocean ecosystems in the 21st century: projections with CMIP5 models, Biogeosciences, 10, 6225–6245, doi:10.5194/bg-10-6225-2013.

Bricaud, A., Babin, M., Morel, A., and Claustre, H.: Variability in the chlorophyll-specific absorption coefficients of natural phytoplankton: analysis and parameterization, J. Geophys. Res., 100, 13321–13332, 1995.

Cheng, L., Trenberth, K. E., Palmer, M. D., Zhu, J., and Abraham, J. P.: Observed and simulated full-depth ocean heat-content changes for 1970–2005, Ocean Sci., 12, 925–935, https://doi.org/10.5194/os-12-925-2016, 2016.

Cocco, V., Joos, F., Steinacher, M., Frölicher, T. L., Bopp, L., Dunne, J., Gehlen, M., Heinze, C., Orr, J., Oschlies, A., Schneider, B., Segschneider, J., and Tjiputra, J. (2013). Oxygen and indicators of stress for marine life in multi-model global warming projections, Biogeosciences, 10, 1849–1868, doi:10.5194/bg-10-1849-2013.

Echevin, V., Hauschildt, J., Colas, F., Thomsen, S., & Aumont, O. (2021). Impact of chlorophyll shading on the Peruvian upwelling system. Geophysical Research Letters, 48, e2021GL094429. https://doi.org/10.1029/2021GL094429

Edwards, A. M., Wright, D. G., Platt, T. (2004) Biological heating effect of a band of phytoplankton. *Journal of Marine Systems*, 49, 89-103. doi: 10.1016/j.jmarsys.2003.05.011.

Edwards, A. M., Platt, T., Wright, D. G. (2001) Biologically induced circulation at fronts. *Journal of geophysical research*, 49, 89-103. doi: 10.1016/j.jmarsys.2003.05.011.

Eppley, R. W.: Temperature and phytoplankton growth in the sea, Fish. Bull., 70, 1063–1085, 1972.

Freing, A., D. W. R. Wallace, and H. W. Bange, 2012: Global oceanic production of nitrous oxide. Philos. Trans. R. Soc. London Ser. B, **367**, 1245–1255.

Garcia, H. E., R. A. Locarnini, T. P. Boyer, J. I. Antonov, O.K. Baranova, M.M. Zweng, J.R. Reagan, D.R. Johnson, (2014). World Ocean Atlas 2013, Volume 3: Dissolved Oxygen, Apparent Oxygen Utilization, and Oxygen Saturation. S. Levitus, Ed., A. Mishonov Technical Ed.; NOAA Atlas NESDIS 75, 27 pp.

Gildor, H., and N. H. Naik (2005), Evaluating the effect of interannual variations of surface chlorophyll on upper ocean temperature, J. Geophys. Res., 110, C07012, doi:10.1029/2004JC002779.

Gnanadesikan, A., and W. G. Anderson (2009), Ocean water clarity and the ocean general circulation in a coupled climate model, J. Phys. Ocean., 39, 314–332.

Good, S. A., M. J. Martin and N. A. Rayner, (2013). EN4: quality controlled ocean temperature and salinity profiles and monthly objective analyses with uncertainty estimates, Journal of Geophysical Research: Oceans, doi:10.1002/2013JC009067

Hajima, T., Watanabe, M., Yamamoto, A., Tatebe, H., Noguchi, M. A., Abe, M., Ohgaito, R., Ito, A., Yamazaki, D., Okajima, H., Ito, A., Takata, K., Ogochi, K., Watanabe, S., and Kawamiya, M. (2020). Development of the MIROC-ES2L Earth system model and the evaluation of biogeochemical processes and feedbacks, Geosci. Model Dev., 13, 2197–2244, https://doi.org/10.5194/gmd-13-2197-2020.

Heinze, C., T. Blenckner, H. Martins, D. Rusiecka, R. Döscher, M. Gehlen, N. Gruber, E. Holland, Ø. Hov, F. Joos, J. B. R. Matthews, R. Rødven and S. Wilson (2021). The quiet crossing of ocean tipping points, Proceedings of the National Academy of Sciences, 118 (9) e2008478118; DOI: 10.1073/pnas.2008478118

Hernandez, O., J. Jouanno, V. Echevin, and O. Aumont (2017), Modification of sea surface temperature by chlorophyll concentration in the Atlantic upwelling systems, J. Geophys. Res. Oceans, 122, 5367–5389, doi:10.1002/2016JC012330.

Hutchins, D.A., Capone, D.G. The marine nitrogen cycle: new developments and global change. Nat Rev Microbiol (2022). https://doi-org.insu.bib.cnrs.fr/10.1038/s41579-022-00687-z

Ilyina, T., K. D. Six, J. Segschneider, E. Maier-Reimer, H. Li, and I. Núñez-Riboni (2013), Global ocean biogeochemistrymodel HAMOCC: Model architecture and performance as component of the MPI-Earth system model in different CMIP5 experimental realizations,J.Adv.Model.EarthSyst.,5, 287–315, doi:10.1029/2012MS000178.

IPCC: Summary for Policymakers, in: IPCC Special Report on the Ocean and Cryosphere in a Changing Climate, edited by: Pörtner,H.-O., Roberts, D.C., Masson-Delmotte, V., Zhai, P., Tignor, M., Poloczanska, E., Mintenbeck, K., Nicolai, M., Okem, A., Petzold, J., Rama, B., and Weyer, N., 2019.

Ji, Q., A. R. Babbin, A. Jayakumar, S. Oleynik, and B. B. Ward (2015), Nitrous oxide production by nitrification and denitrification in the Eastern Tropical South Pacific oxygen minimum zone, Geophys. Res. Lett., 42, 10,755–10,764, doi:10.1002/2015GL066853.

Ji, Q., Buitenhuis, E., Suntharalingam, P., Sarmiento, J. L., & Ward, B. B. (2018). Global nitrous oxide production determined by oxygen sensitivity of nitrification and denitrification. Global Biogeochemical Cycles, 32, 1790–1802. https://doi.org/10.1029/2018GB005887

Kahru, M., Leppaenen, J.-M., and Rud, O. (1993). Cyanobacterial blooms cause heating of the sea surface, Mar. Ecol.-Prog. Ser., 101, 1–7.

Kolodziejczyk, N., W. Llovel, and E. Portela (2019). Interannual variability of upper ocean water masses as inferred from Argo Array, Journal of Geophysical Research: Oceans. doi:10.1029/2018JC014866.

Kolodziejczyk, N., A. Prigent-Mazella and F. Gaillard (2021). ISAS temperature and salinity gridded fields. SEANOE. https://doi.org/10.17882/52367

Kortzinger, A., Hedges, J. I., and Quay, P. D.: Redfield ratios revisited: removing the biasing effect of anthropogenic CO2, Limnol. Oceanogr., 46, 964–970, 2001.

Kwiatkowski, L., Torres, O., Bopp, L., Aumont, O., Chamberlain, M., Christian, J. R., Dunne, J. P., Gehlen, M., Ilyina, T., John, J. G., Lenton, A., Li, H., Lovenduski, N. S., Orr, J. C., Palmieri, J., Santana-Falcón, Y., Schwinger, J., Séférian, R., Stock, C. A., Tagliabue, A., Takano, Y., Tjiputra, J., Toyama, K., Tsujino, H., Watanabe, M., Yamamoto, A., Yool, A., and Ziehn, T.: Twenty-first century ocean warming, acidification, deoxygenation, and upper-ocean nutrient and primary production decline from CMIP6 model projections, Biogeosciences, 17, 3439–3470, https://doi.org/10.5194/bg-17-3439-2020, 2020.

Lam, P., and M. Kuypers (2011). Microbial Nitrogen Cycling Processes in Oxygen Minimum Zones, Annual Review of Marine Science 3:1, 317-345, doi:10.1146/annurev-marine-120709-142814

Large, W. G., and S. Yeager (2009). The global climatology of an interannually varying air-sea ux data set, Clim. Dyn., 33, 341–364, doi:10.1007/s00382-008-0441-3.

Lengaigne, M., G. Madec, L. Bopp, C. Menkes, O. Aumont, and P. Cadule (2009). Bio-physical feedbacks in the Arctic Ocean using an Earth system model, Geophys. Res. Lett., 36, L21602, doi:10.1029/2009GL040145.

Lengaigne, M., Menkes, C., Aumont, O. et al. Influence of the oceanic biology on the tropical Pacific climate in a coupled general circulation model. Clim. Dyn., 28**,** 503–516 (2007). https://doi.org/10.1007/s00382-006-0200-2

Levitus, S., J. I. Antonov, T. P. Boyer, O. K. Baranova, H. E. Garcia, R. A. Locarnini, A.V. Mishonov, J. R. Reagan, D. Seidov, E. S. Yarosh, M. M. Zweng, (2012): World Ocean heat content and thermosteric sea level change (0-2000 m) 1955-2010. Geophys. Res. Lett. , 39, L10603, doi:10.1029/2012GL051106

Liang, X., Liu, C. R., Ponte, M., and Chambers, D. P. (2021). A Comparison of the Variability and Changes in Global Ocean Heat Content from Multiple Objective Analysis Products During the Argo Period, J. Climate, 34(19), 7875–7895, https://doi.org/10.1175/JCLID-20-0794.1.

Llovel, W. and L. Terray (2016). Observed southern upper-ocean warming over 2005–2014 and associated mechanisms, Environ. Res. Lett., 11, 124023.

Llovel, W., N. Kolodziejczyk, S. Close, T. Penduff, J.-M. Molines and L. Terray (2022). Imprint of intrinsic ocean variability on decadal trends of regional sea level and ocean heat content using synthetic profiles, Environ. Res. Lett., 17, 044063.

Locarnini, R. A., A. V. Mishonov, J. I. Antonov, T. P. Boyer, H. E. Garcia, O. K. Baranova, M. M. Zweng, C. R. Paver, J. R. Reagan, D. R. Johnson, M. Hamilton, and D. Seidov, (2013). World Ocean Atlas 2013, Volume 1: Temperature. S. Levitus, Ed., A. Mishonov Technical Ed.; NOAA Atlas NESDIS 73, 40 pp.

Löptien, U., C. Eden, A. Timmermann, and H. Dietze (2009), Effects of biologically induced differential heating in an eddy-permitting coupled ocean-ecosystem model, J. Geophys. Res., 114, C06011, doi:10.1029/2008JC004936.

Lyman, J., Good, S., Gouretski, V. et al. Robust warming of the global upper ocean. Nature **465,** 334–337 (2010). https://doi.org/10.1038/nature09043

Madec, G. (2008). Nemo ocean engine. Note du Pôle de modélisation de l'Institut Pierre-Simon Laplace, 27, 1–217.

Maes, C., and T. J. O'Kane (2014), Seasonal variations of the upper ocean salinity stratification in the Tropics, J. Geophys. Res. Oceans, 119, 1706–1722, doi:10.1002/2013JC009366.

Manizza, M., C. Le Quéré, A. J. Watson, and E. T. Buitenhuis (2005), Bio-optical feedbacks among phytoplankton, upper ocean physics and sea-ice in a global model, Geophys. Res. Lett., 32, L05603, doi:10.1029/2004GL020778.

Manizza, M., C. Le Quéré, A. J. Watson, and E. T. Buitenhuis (2008), Ocean biogeochemical response to phytoplankton-light feedback in a global model, J. Geophys. Res., 113, C10010, doi:10.1029/2007JC004478.

Martinez-Rey, J., Bopp, L., Gehlen, M., Tagliabue, A., and Gruber, N.: Projections of oceanic N_2O emissions in the 21st century using the IPSL Earth system model, Biogeosciences, 12, 4133–4148, https://doi.org/10.5194/bg-12-4133-2015, 2015.

Marzeion, B., Timmermann, A., Murtugudde, R., & Jin, F. (2005). Biophysical Feedbacks in the Tropical Pacific, Journal of Climate, 18(1), 58-70.

Meyssignac B, Boyer T, Zhao Z, Hakuba MZ, Landerer FW, Stammer D, Köhl A, Kato S, L'Ecuyer T, Ablain M, Abraham JP, Blazquez A, Cazenave A, Church JA, Cowley R, Cheng L, Domingues CM, Giglio D, Gouretski V, Ishii M, Johnson GC, Killick RE, Legler D, Llovel W, Lyman J, Palmer MD, Piotrowicz S, Purkey SG, Roemmich D, Roca R, Savita A, von Schuckmann K, Speich S, Stephens G, Wang G, Wijffels SE and Zilberman N (2019)

Measuring Global Ocean Heat Content to Estimate the Earth Energy Imbalance. Front. Mar. Sci. 6:432. doi: 10.3389/fmars.2019.00432

Mignot, J., D. Swingedouw, J. Deshayes, O. Marti, C. Talandier, R. Séférian, M. Lengaigne, G. Madec (2013). On the evolution of the oceanic component of the IPSL climate models from CMIP3 to CMIP5: A mean state comparison, Ocean Modelling, Volume 72, Pages 167-184, ISSN 1463-5003, https://doi.org/10.1016/j.ocemod.2013.09.001.

Morel A (1988) Optical modeling of the upper ocean in relation to its biogenous matter content (Case I waters). J Geophys Res 93:10749–10768

Morel, A. and J.-F. Berthon, 1989 : Surface pigments, algal biomass profiles, and potential production of the euphotic layer : Relationships reinvestigated in view of remote-sensing applications. Limnol. Oceanogr., 34(8), 1545–1562.

Morel A, and Maritorena S (2001) Bio-optical properties of oceanic waters: a reappraisal. J Geophys Res 106:7163–7180

Murtugudde, R., Beauchamp, J., McClain, C. R., Lewis, M., & Busalacchi, A. J. (2002). Effects of Penetrative Radiation on the Upper Tropical Ocean Circulation, Journal of Climate, 15(5), 470-486.

Myhre, G., D. Shindell, F.-M. Bréon, W. Collins, J. Fuglestvedt, J. Huang, D. Koch, J.-F. Lamarque, D. Lee, B. Mendoza, T. Nakajima, A. Robock, G. Stephens, T. Takemura and H. Zhang, (2013). Anthropogenic and Natural Radiative Forcing. In: Climate Change 2013: The Physical Science Basis. Contribution of Working Group I to the Fifth Assessment Report of the Intergovernmental Panel on Climate Change [Stocker, T.F., D. Qin, G.-K. Plattner, M. Tignor, S.K. Allen, J. Boschung, A. Nauels, Y. Xia, V. Bex and P.M. Midgley (eds.)]. Cambridge University Press, Cambridge, United Kingdom and New York, NY, USA.

Nakamoto, S., S. P. Kumar, J. M. Oberhuber, J. Ishizaka, K. Muneyama, and R. Frouin (2001), Response of the equatorial Pacific to chlorophyll pigment in a mixed layer isopycnical ocean general circulation model, Geophys. Res. Lett., 28, 2021– 2024.

Oschlies, A. (2004), Feedbacks of biotically induced radiative heating on upper-ocean heat budget, circulation, and biological production in a coupled ecosystem-circulation model, J. Geophys. Res., 109, C12031, doi:10.1029/2004JC002430.

Park, JY., Kug, JS., Seo, H. et al. Impact of bio-physical feedbacks on the tropical climate in coupled and uncoupled GCMs. Clim Dyn **43,** 1811–1827 (2014). https://doi.org/10.1007/s00382-013-2009-0

Patara, L., Vichi, M., Masina, S. et al. Global response to solar radiation absorbed by phytoplankton in a coupled climate model. Clim Dyn **39,** 1951–1968 (2012). https://doi.org/10.1007/s00382-012-1300-9

Ravishankara, A. R., J. S. Daniel, and R. W. Portmann, 2009: Nitrous oxide (N2O): The dominant ozone-depleting substance emitted in the 21st century. Science, **326**, 123–125.

Roemmich, D., and J. Gilson, 2009: The 2004–2008 mean and annual cycle of temperature, salinity, and steric height in the global ocean from the Argo Program. Prog. Oceanogr., 82, 81–100, https://doi.org/10.1016/j.pocean.2009.03.004.

Sallée, JB., Pellichero, V., Akhoudas, C. *et al.* Summertime increases in upper-ocean stratification and mixed-layer depth. Nature 591**,** 592–598 (2021). https://doi.org/10.1038/s41586-021-03303-x

Schmidtko, S., Stramma, L. & Visbeck, M. Decline in global oceanic oxygen content during the past five decades. Nature 542, 335–339 (2017).

Séférian, R., Berthet, S., Yool, A. et al. Tracking Improvement in Simulated Marine Biogeochemistry Between CMIP5 and CMIP6. Curr Clim Change Rep **6,** 95–119 (2020). https://doi.org/10.1007/s40641-020-00160-0

Séférian, R., Nabat, P., Michou, M., Saint-Martin, D., Voldoire, A., Colin, J., et al (2019). Evaluation of CNRM Earth-System model, CNRM-ESM2-1: role of Earth system processes in present-day and future climate. Journal of Advances in Modeling Earth Systems, 11. https://doi.org/10.1029/2019MS001791

Sweeney, C., Gnanadesikan, A., Griffies, S. M., Harrison, M. J., Rosati, A. J., & Samuels, B. L. (2005). Impacts of Shortwave Penetration Depth on Large-Scale Ocean Circulation and Heat Transport, Journal of Physical Oceanography, 35(6), 1103-1119.

Takahashi, T., Broecker, W. S., and Langer, S.: Redfield ratio based on chemical data from isopycnal surfaces, J. Geophys. Res., 90, 6907–6924, 1985.

Tian, H., Xu, R., Canadell, J.G., R. L. Thompson, W. Winiwarter, P. Suntharalingam, E. A. Davidson, P. Ciais, R. B. Jackson, G. Janssens-Maenhout, M. J. Prather, P. Regnier, N. Pan, S. Pan, G. Peters, H. Shi, F. N. Tubiello, S. Zaehle, F. Zhou, A. Arneth, G. Battaglia, S. Berthet, L. Bopp, A. F. Bouwman, E. T. Buitenhuis, J. Chang, Martyn P. Chipperfield, S. R.S. Dangal, E. Dlugokencky, J. Elkins, Bradley D. Eyre, B. Fu, B. Hall, A. Ito, F. Joos, P. B. Krummel, A. Landolfi, G. G. Laruelle, R. Lauerwald, W. Li, S. Lienert, T. Maavara, M. MacLeod, D. B. Millet, S. Olin, P. K. Patra, R. G. Prinn, P. A. Raymond, D. J. Ruiz, Guido R. van der Werf, N. Vuichard, J. Wang, R. Weiss, K. C. Wells, C. Wilson, J. Yang and Y. Yao (2020). A comprehensive quantification of global nitrous oxide sources and sinks. Nature 586, 248–256. https://doi.org/10.1038/s41586-020-2780-0.

Tiano, L., E. Garcia-Robledo, T. Dalsgaard, A. H. Devol, B. B. Ward, O. Ulloa, D. E. Canfield, N. P. Revsbech (2014). Oxygen distribution and aerobic respiration in the north and south eastern tropical Pacific oxygen minimum zones. Deep Sea Research Part I: Oceanographic Research Papers, Volume 94, Pages 173-183, https://doi.org/10.1016/j.dsr.2014.10.001.

Timmermann, A., and F.-F. Jin, 2002. Phytoplankton influences on tropical climate, Geophys. Res. Lett., 29(23), 2104, doi:10.1029/2002GL015434.

Tsujino, H., Urakawa, S., Nakano, H., Small, R. J., Kim, W. M., Yeager, S. G., Danabasoglu, G., Suzuki, T., Bamber J. L., Bentsen, M., Böning, C. W., Bozec, A., Chassignet, E. P., Curchitser, E., Boeira Dias, F., Durack, P. J., Griffies, S. M., Harada, Y., Ilicak, M., Josey, S. A., Kobayashi, C., Kobayashi, S., Komuro, Y., Large, W. G., Le Sommer, J., Marsland, S. J., Masina, S., Scheinert, M., Tomita, H., Valdivieso, M., and Yamazaki, D. (2018). JRA-55 based surface dataset for driving ocean–sea-ice models (JRA55-do), Ocean Model., 130, 79–139, https://doi.org/10.1016/j.ocemod.2018.07.002.

Tsujino, H., Urakawa, L. S., Griffies, S. M., Danabasoglu, G., Adcroft, A. J., Amaral, A. E., Arsouze, T., Bentsen, M., Bernardello, R., Böning, C. W., Bozec, A., Chassignet, E. P., Danilov, S., Dussin, R., Exarchou, E., Fogli, P. G., Fox-Kemper, B., Guo, C., Ilicak, M., Iovino, D., Kim, W. M., Koldunov, N., Lapin, V., Li, Y., Lin, P., Lindsay, K., Liu, H., Long, M. C., Komuro, Y., Marsland, S. J., Masina, S., Nummelin, A., Rieck, J. K., Ruprich-Robert, Y., Scheinert, M., Sicardi, V., Sidorenko, D., Suzuki, T., Tatebe, H., Wang, Q., Yeager, S. G., and Yu, Z. (2020). Evaluation of global ocean–sea-ice model simulations based on the experimental protocols of the Ocean Model Intercomparison Project phase 2 (OMIP-2), Geosci. Model Dev., 13, 3643–3708, https://doi.org/10.5194/gmd-13-3643-2020, 2020.

Uitz, J., Claustre, H., Morel, A., and Hooker, S. B. (2006), Vertical distribution of phytoplankton communities in open ocean: An assessment based on surface chlorophyll, *J. Geophys. Res.*, 111, C08005, doi:10.1029/2005JC003207.

Valente, A, Sathyendranath, S, Brotas, V, Groom, S, Grant, M, Taberner, M, Antoine, D, Arnone, R, Balch, W, Barker, K, Barlow, R, Bélanger, S, Berthon, JF, Besiktepe, S, Brando, V, Canuti, E, Chavez, F, Claustre, H, Crout, R, Frouin, R, Garcìa-Soto, C, Gibb, SW, Gould, R, Hooker, S, Kahru, M, Klein, H, Kratzer, S, Loisel, H, McKee, D, Mitchell, BG, Moisan, T, Muller-Karger, F., O'Dowd, L, Ondrusek, M, Poulton, A, Repecaud, M, Smyth, T, Sosik, HM, Twardowski, M, Voss, K, Werdell, J, Wernand, M, Zibordi, G (**2016**) A compilation of global bio-optical in situ data for ocean-colour satellite applications. Earth Syst. Sci. Data, 8, 235–252, doi: 10.5194/essd-8-235-2016

Wanninkhof, R. (1992). Relationship between wind speed and gas exchange over the ocean, J. Geophys. Res., 97, 7373–7382, doi:10.1029/92JC00188.

Wanninkhof, Rik, (2014), Relationship between wind speed and gas exchange over the ocean revisited, Limnol. Oceanogr. Methods, 12, doi:10.4319/lom.2014.12.351.

Weiss, R. F., and B. A. Price (1980). Nitrous oxide solubility in water and seawater Marine Chemistry, Volume 8, Issue 4, Pages 347-359; DOI: 10.1016/0304-4203(80)90024-9

Wilson, S. T., Al-Haj, A. N., Bourbonnais, A., Frey, C., Fulweiler, R. W., Kessler, J. D., Marchant, H. K., Milucka, J., Ray, N. E., Suntharalingam, P., Thornton, B. F., Upstill-Goddard, R. C., Weber, T. S., Arévalo-Martínez, D. L., Bange, H. W., Benway, H. M., Bianchi, D., Borges, A. V., Chang, B. X., Crill, P. M., del Valle, D. A., Farías, L., Joye, S. B., Kock, A., Labidi, J., Manning, C. C., Pohlman, J. W., Rehder, G., Sparrow, K. J., Tortell, P. D., Treude, T., Valentine, D. L., Ward, B. B., Yang, S., and Yurganov, L. N.: Ideas and perspectives: A strategic assessment of methane and nitrous oxide measurements in the marine environment, Biogeosciences, 17, 5809–5828, https://doi.org/10.5194/bg-17-5809-2020, 2020.

Yang, S., B. X. Chang, M. J. Warner, T. S. Weber, A. M. Bourbonnais, A. E. Santoro, A. Kock, R. E. Sonnerup, J. L. Bullister, S. T. Wilson and D. Bianchi (2020). Global reconstruction reduces the uncertainty of oceanic nitrous oxide emissions and reveals a vigorous seasonal cycle, Proceedings of the National Academy of Sciences, 117 (22) 11954-11960; DOI: 10.1073/pnas.1921914117